Rapid Communications

Charge qubit in van der Waals heterostructures

Bruno Lucatto,[1,*] Daniel S. Koda,[1,†] Friedhelm Bechstedt,[2] Marcelo Marques,[1] and Lara K. Teles[1]

[1]*Grupo de Materiais Semicondutores e Nanotecnologia, Instituto Tecnológico de Aeronáutica, DCTA, 12228-900 São José dos Campos, Brazil*

[2]*Institut für Festkörpertheorie und -optik, Friedrich-Schiller-Universität, Max-Wien-Platz 1, D-07743 Jena, Germany*

(Received 27 April 2019; revised manuscript received 12 September 2019; published 27 September 2019)

In this Rapid Communication, we develop the concept of charge qubits in van der Waals heterostructures. A theoretical proof of concept is provided for the $ZrSe_2/SnSe_2$ system, in which a framework connecting the electronic structure with quantum information is described. The quantum state is prepared by applying a vertical electric field, manipulated by short field pulses, and measured via electric currents. The proposed qubit is robust, operational at high temperature, and compatible with two-dimensional material technology, opening different avenues for the field.

DOI: 10.1103/PhysRevB.100.121406

Introduction. The quantum superposition (QS) principle plays a major role in the so-called second generation of quantum technologies, which includes quantum counterparts of cryptography, imaging, computing, and sensing [1]. Preparation, manipulation, and measurement of the QS are central aspects to enable the operation of such advanced devices. The superposition of two quantum states characterizes the unit of quantum information, a qubit, typically implemented by two-level systems [2], polarizations of light [3], or electron spin orientations [4]. However, creating practical qubits that are both isolated from the environment and controllable by external means is still a major challenge in the field [5]. Therefore, the advance of quantum computation requires new ways to implement qubits, and innovative systems are indispensable for integrable and scalable qubit technology [6–8]. Recently, along with the strong development of two-dimensional (2D) material technology and their van der Waals heterostructures (vdWHs) [9–11], progress has been made to find possible candidates for qubits in monolayer [12] and multilayer [13–15] structures.

Despite the weak interaction between the two atomic layers in such a 2D heterostructure, if the band structures of the isolated sheets are nearly aligned on an absolute energy scale, QS can arise from wave functions localized in different layers but forming the conduction or valence bands of the heterostructure [16]. Bonding and antibonding combinations of orbitals localized on each subsystem build the basis functions of the joint conduction or valence band [17]. The resulting energy splittings and mixing coefficients of the wave functions depend on the vdW interlayer distance and the natural band discontinuities [16]. The mixing coefficients characterize the quantum-mechanical probabilities to find a certain carrier, electron, or hole, in each of the two 2D materials of the heterostructure. However, despite the fact that the QS property in 2D vdWHs is highly promising, it has not yet been explored for qubit applications.

In this Rapid Communication, we provide a qubit concept based on a quantum spatial superposition of an electron between the two sheets of a gated vdWH. By combining *ab initio* calculations and quantum information theory, we demonstrate a complementarity between orbital compositions of the heterostructure conduction band as a function of the gate field. A framework connecting electronic structure calculations with quantum information methods is developed to bridge between both representations. The example of the $ZrSe_2/SnSe_2$ bilayer is thoroughly investigated as a proof of concept. Our results highlight a different pathway for implementing qubits—not only due to the further developments over the bilayer here proposed but also due to the myriad potential combinations of 2D materials. Moreover, the present work will boost both theoretical and experimental efforts on the study of the related phenomena.

Computational details. The structural and electronic properties are calculated using the density functional theory (DFT) as implemented in the Vienna *ab initio* simulation package (VASP) [18]. The wave functions and pseudopotentials are generated within the projector augmented-wave (PAW) method [19]. Exchange and correlation (XC) are described using the Perdew-Burke-Ernzerhof (PBE) functional within the generalized gradient approximation (GGA) [20]. The van der Waals interaction is taken into account using the optB86b functional [21]. Integrations over the 2D Brillouin zone (BZ) are performed using an $11 \times 11 \times 1$ Γ-centered Monkhorst-Pack $\vec{k}$-point mesh [22] for 1×1 lateral unit cells. The repeated slab method is applied to simulate individual 2D crystals as well as their heterocombinations [23]. Minimum lateral unit cells employed are found within the coincidence lattice method [24]. To account for the excitation aspect we apply the XC hybrid functional of Heyd-Scuseria-Ernzerhof (HSE06) [25–27]. More detailed information is given in the Supplemental Material [28].

Effect of vertical electric field on band structure. To illustrate the superposition of states for electrons and holes in

*brunolucatto@gmail.com; gmsn@ita.br

†Present address: Department of Materials Science and Engineering, Massachusetts Institute of Technology, Cambridge, MA 02139.

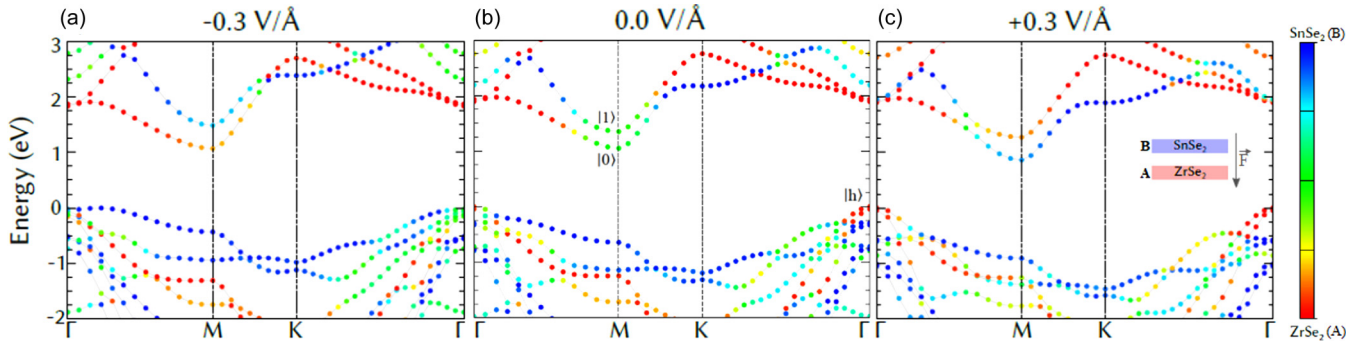

FIG. 1. Band structures of $ZrSe_2/SnSe_2$ heterostructure with applied vertical electric field of (a) -0.3 V/Å, (b) 0.0 V/Å, and (c) $+0.3$ V/Å. The inset in (c) shows the positive field orientation is considered from the $SnSe_2$ layer to the $ZrSe_2$ layer. The color of the marker represents the relative contribution of each monolayer to the eigenvalue. The VBM is chosen as energy zero.

biased 2D vdWHs, we start with a model system consisting of $ZrSe_2$ and $SnSe_2$ transition-metal dichalcogenide monolayers. Because of the near lattice match, 1×1 cells with zero twist and a small antisymmetric biaxial strain of $\pm 0.8\%$ are chosen [17]. A vertical electric field $\vec{F}$ simulates that the heterostructure is gated or vertically biased as displayed in the inset of Fig. 1(c). The band structures resulting for three field strengths are plotted in Fig. 1 along with high-symmetry directions in the Brillouin zone (BZ) for a small energy interval around the fundamental gap. The indirect semiconductor character with the conduction-band minimum (CBM) at M and the valence-band maximum (VBM) at Γ is conserved for all field strengths. In Fig. 1, the color of each eigenvalue represents the relative contribution of each crystal to the wave function. It is obtained as the proportion of the projections of the Kohn-Sham orbitals onto the atomic orbitals (i.e., the orbital character of these levels [29]) for all the atoms in each material. In this work, the two-level system of the qubit is defined by the first and second lowest conduction states at the M point in the BZ, which are denoted by $|0\rangle$ and $|1\rangle$, respectively. The hybridization is also present in other states at the band edges, which may impact measures of carrier concentration. In this sense, we also include in the following analysis the hole state in the VBM at Γ, denoted by $|h\rangle$. These band states are composed by wave functions localized at one of the 2D crystals. Figure 1 clearly shows that their contribution can be manipulated by an external field $\vec{F}$.

In the unbiased case [Fig. 1(b)], $|0\rangle$ and $|1\rangle$ have almost equal contributions of each layer of the heterojunction, as indicated by the green dots. In the absence of an electric field, an electron in one of these states tends to be in an electronic state with equal probabilities to find the carrier in material A or B. Instead, in the biased case, the conduction-band states are given by superpositions of the wave functions that belong to material A or to material B with different weights. This behavior is different from what happens at the top valence-band state. The character of $|h\rangle$ is predominantly from A, as indicated by the red color of the VBM in Fig. 1(b). Therefore, a hole tends to be localized in crystal A.

An external electric field in the stacking direction of the vdWH can shift the bands of the crystals with respect to each other, as indicated in Figs. 1(a) and 1(c). The corresponding change in energy also impacts the overlap of the orbitals, thus affecting their relative contribution to the bilayer wave function. By applying an electric field in the B-A direction, as indicated by the inset in Fig. 1(c), electrons at $|0\rangle$ are lowered in energy. The electric field then shifts down the band structure of material B relatively to the band structure of material A, consequently letting $|0\rangle$ be a state with a stronger character of material B, as indicated by Fig. 1(c). As $|0\rangle$ becomes more localized at B, $|1\rangle$ and $|h\rangle$ becomes more localized at A.

The opposite holds true when we apply an electric field in the reverse direction: The bands of material B are shifted toward the vacuum level, allowing $|0\rangle$ to be more localized at A and $|1\rangle$ more localized at B, as indicated in Fig. 1(a). However, this is not the only effect observed in this case. Since the band structure of material B is shifted toward higher absolute energies, the VBM of material B starts to line up with the VBM of material A, and thus $|h\rangle$ exhibits a stronger hybridization and nearly equal contributions from both sheets A and B, as indicated by the colors of Fig. 1(a). Moreover, for this extreme field situation, the VBM is slightly shifted from Γ, which is not true for the intermediate values (see the Supplemental Material for a more detailed discussion on hole states [28]).

There is a complementarity between $|0\rangle$ and $|1\rangle$ under the influence of the gate field, where one state becomes more localized in one sheet as the other becomes more localized in the other sheet. Therefore, an electron occupying any superposition of the two states localized in different sheets configures a charge qubit in the AB heterostructure, where for strong positive electric fields the $|0\rangle$ and $|1\rangle$ states are localized in sheets B and A, respectively, and the opposite happens for strong negative electric fields. The corresponding energy configuration is illustrated schematically in Fig. 2 as a function of the electric field. An anticrossing energy $\Delta_{ac} = 0.30$ eV is determined by the difference between the eigenenergies E_1 and E_0 of the band states $|1\rangle$ and $|0\rangle$, respectively, for an electric field, where the layer contributions are equal. This energy difference corresponds to a frequency $f \approx 70$ THz. In the studied system, this occurs at nearly vanishing field $F_{ac} \approx -15$ mV/Å, as depicted in Figs. 2 and 3. The conduction-level system, therefore, has similarities with the electronic structure of the charge qubit in a double quantum dot [30,31].

The contribution of each layer A or B to the Bloch wave function of the states $|0\rangle$ and $|1\rangle$ in the AB heterostructure strongly depends on the electric field strength F. Thus, an

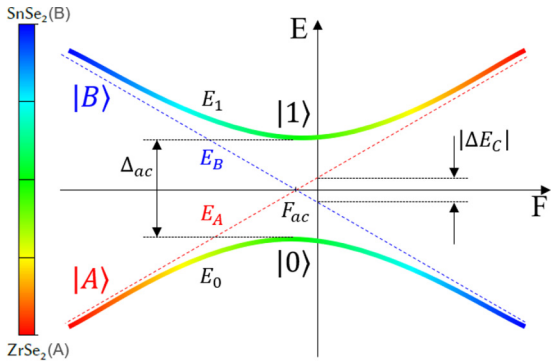

FIG. 2. Conduction-band energy-level diagram vs gate-field strength F formed by the localized electron states for an uncoupled system $|A\rangle$ and $|B\rangle$ (dashed lines) with eigenenergies E_A and E_B, respectively. The hybridization of the states for the coupled system results in new eigenstates $|0\rangle$ and $|1\rangle$, with eigenenergies E_0 and E_1, respectively, and anticrossing energy Δ_{ac} (solid lines). For strong fields the qubit eigenstates are well approximated by $|A\rangle$ and $|B\rangle$, but for field values around F_{ac} the eigenstates are strongly delocalized. For the zero field, the energy difference $E_B - E_A = \Delta E_C$ characterizes the conduction-band discontinuity.

electron wave function $|\psi(F)\rangle$ of the AB heterostructure is mainly a combination of the corresponding wave functions $|A\rangle$ and $|B\rangle$ of the two individual atomic sheets with different weights. It can be written as a superposition for a given field strength F,

$$|\psi(F)\rangle = \alpha_\psi(F)|A\rangle + \beta_\psi(F)|B\rangle, \tag{1}$$

with complex coefficients. Because of the relatively large distance between the sheets, we consider the overlap of these states to be small, such that the normalization of the coefficients is given by $|\alpha_\psi(F)|^2 + |\beta_\psi(F)|^2 = 1$. Under this approximation, $|A\rangle$ and $|B\rangle$ are orthogonal and, therefore, the

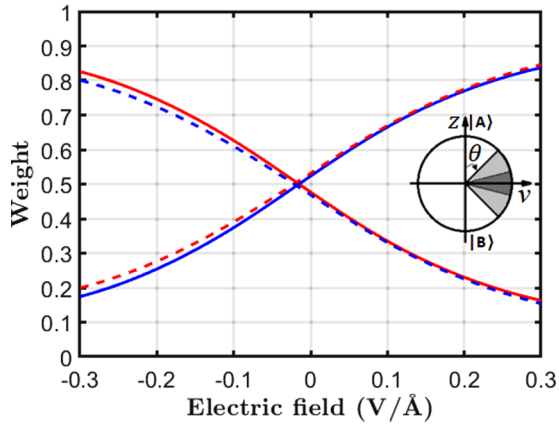

FIG. 3. Weights $|\alpha_\psi|^2$ (red) and $|\beta_\psi|^2$ (blue), for $|\psi\rangle$ equals $|0\rangle$ (solid lines) and $|1\rangle$ (dashed lines), as a function of the applied vertical electric field. The inset represents the area of the Bloch sphere in the A/B basis in which $|0\rangle$ and $|1\rangle$ are comprised for the considered electric fields ($|F| < 0.3$V/Å) (light gray), and for small fields ($|F| < 0.1$V/Å) (dark gray) considering a generic azimuthal angle ϕ. The horizontal axis indicates the direction of the vector $\hat{v} = \cos\phi\hat{x} + \sin\phi\hat{y}$ in the xy plane.

squared moduli of their coefficients give the weights of each sheet to the wave function, as illustrated in Fig. 3. This figure also provides evidence for the complementarity between $|0\rangle$ and $|1\rangle$, which further justifies the usage of the system as a charge qubit realized in the sheet arrangement.

The representation (1) can be also interpreted as a coherent superposition of basic quantum states $|A\rangle$ and $|B\rangle$ at a given time or field strength, where the probability amplitudes α_ψ, β_ψ to find an electron characterize a linear combination as in a single qubit [32]. In a linear approximation around the state of maximum delocalization, considering $F_{ac} \approx 0$, one finds for the biased $ZrSe_2/SnSe_2$ heterostructure,

$$\begin{Bmatrix} |\alpha_0(F)|^2 \\ |\beta_0(F)|^2 \end{Bmatrix} = \begin{Bmatrix} |\beta_1(F)|^2 \\ |\alpha_1(F)|^2 \end{Bmatrix} = \frac{1 \mp 2.9F}{2} \ (F \text{ in V/Å}). \tag{2}$$

The states $|\psi(F)\rangle$ of Eq. (1) can be described as a Bloch vector in the standard Bloch sphere representation, where the mixing coefficients are described by spherical coordinates with angles θ and ϕ as

$$\begin{aligned} \alpha &= \cos(\theta/2), \\ \beta &= e^{i\phi}\sin(\theta/2). \end{aligned} \tag{3}$$

The polar angle θ can be calculated as

$$\theta = 2\arccos(|\alpha|) = 2\arcsin(|\beta|). \tag{4}$$

For the considered values of the electric field, the Bloch vector lies in the shaded area depicted in the inset of Fig. 3, which corresponds to the interval between $\theta \approx 45^\circ$ and $\theta \approx 135^\circ$. Considering $|F| < 0.1$ V/Å, the linear approximation introduces a small error, and the vector lies in the dark gray area in the inset of Fig. 3.

Usage as a qubit. A general superposition state $|\psi\rangle$ on the described two-level system for a given field F can be expanded in the energy eigenvector basis $\{|0\rangle, |1\rangle\}$ as $|\psi\rangle = \xi|0\rangle + \eta|1\rangle$. Writing the energy eigenvectors in the A/B basis, $|0\rangle = \alpha_0|A\rangle + \beta_0|B\rangle$ and $|1\rangle = \alpha_1|A\rangle + \beta_1|B\rangle$, we find that $|\psi\rangle$ in this basis is written as $|\psi\rangle = \alpha_\psi|A\rangle + \beta_\psi|B\rangle$, where

$$\begin{aligned} \alpha_\psi &= \xi\alpha_0 + \eta\alpha_1, \\ \beta_\psi &= \xi\beta_0 + \eta\beta_1. \end{aligned} \tag{5}$$

A possible application of the two-level system as a quantum bit is to initialize the system in the desired state, by choosing a suitable electric field strength and allowing the system to relax to ensure the electron is in the lowest CBM, i.e., in state $|0\rangle$. In order to apply single-qubit quantum gates, the gate field is set to another value, thus changing the two-level system's Hamiltonian itself, since it is a function of the field strength F. If this change is made within a slow process, the coefficients of the energy eigenvectors' basis ξ and η would stay constant throughout the process, under the conditions of the adiabatic theorem. Therefore, the electron would stay in state $|0\rangle$, regardless of the wave function of $|0\rangle$ being different from the starting one, which implies that α_ψ and β_ψ are changed. On the other hand, if the variation of the electric field is fast enough, the electron wave function would be approximately unchanged during the whole process, i.e., α_ψ and β_ψ would be constant. Together with the fact that the

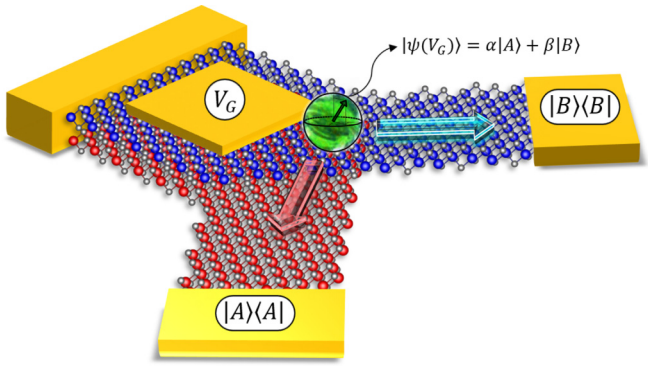

FIG. 4. Schematic representation of a possible physical implementation of the qubit. The electrode V_G applies the field on the stacking direction, changing the state $|\psi(V_G)\rangle$ of the electron in the conduction band, represented by the green Bloch sphere. By inducing a drift in the horizontal direction, the electron wave function will collapse in one of the two electrodes of the isolated portion of the sheets ($|A\rangle\langle A|$ or $|B\rangle\langle B|$), with the probability depending on its localization in each sheet. The Zr, Sn, and Se atoms are represented in red, blue, and gray, respectively.

coefficients of the energy eigenstates in the A/B basis change with the electric field, this implies that ξ and η change. This behavior opens the possibility of moving the electron to the excited state without recurring to optical excitations. In order to measure the resulting state, the carrier concentrations in each sheet must be measured in a time window and compared to each other.

A general control technique applicable to the vdW qubit has already been proposed in Ref. [33], where the tunneling through the forbidden crossing is modeled, and the possibility of performing general rotations in the Bloch sphere is demonstrated. The readout of the qubit can be achieved by applying an additional external bias in the horizontal direction in each sheet and, thus, inducing a small carrier drift. By measuring the resulting currents, the carrier concentration in the layers can be deduced. A possible structure for the device that would allow for the operations here described is depicted in Fig. 4. Multiqubit coupling is necessary for the implementation of two-qubit gates, and we believe that it can be achieved between two adjacent heterostructures, with individual gates (see the Supplemental Material for a schematic image [28]). The state of each individual qubit would be manipulated as described, and tunneling between the adjacent layers would couple them.

Since the variation of the orbital character of a band is continuous with respect to the crystal momentum (see Fig. 1), even if more than one electron is excited, we can assume that it will have approximately the same mixing coefficients as the first one. The Pauli exclusion principle is satisfied due to the difference in the crystal momentum quantum number. Therefore, it may be possible to perform the same operation with many electrons at the same time, if the decoherence time does not decrease too much due to carrier collisions. This would allow for a single measurement operation, since the desired statistics of the results would be given by the relative amplitude between the currents flowing through each sheet. Experimental realization of the qubit should provide a measure of how the (electro)chemical potential position affects the decoherence time. Besides, since $\Delta_{ac} \gg k_B T$, where k_B is the Boltzmann constant and T is the room temperature, we expect the system to operate around room temperature.

It is worth emphasizing that the described vdW charge qubit is not restricted to the studied system. Instead, due to the fact that there are several possible combinations of 2D materials, it is highly probable that other similar systems exist. Considering that there is a practical limit to the intensity of electric fields that can be applied, which also limits how much bands can be shifted with respect to each other, a first filter to predict vdW combinations that may present QS is by analyzing their natural band alignments, as in Anderson's rule [34]. A prediction for a list of monolayers is presented in the Supplemental Material [28] (see also Ref. [35] therein). However, for a real prediction, one needs to go further and make electronic structure calculations, since the desired hybridization effect depends not only on the proximity of the energy levels [16]. Moreover, applying strain on the heterostructure may also lead to hybridization in systems with large natural band discontinuities [17].

Summary. We combined the formalism of quantum information theory and quantitative results obtained through *ab initio* calculations to propose and describe a concept of qubits based on a spatial quantum superposition in vdWHs. For that purpose, we have shown that the minima of the first two conduction bands of the $ZrSe_2/SnSe_2$ vdWH allow for a quantum superposition between states localized in one of the two 2D layers and that this superposition can be accessed and modulated through a gate electric field. A physical device based on this working principle is described. The qubit has the intrinsic qualities of being based on robust electronic states, not requiring low operating temperatures, being directly integrable with electronic devices, measurable through electric currents, and being fully compatible with the existing and well-established technology of 2D materials.

Acknowledgments. The authors thank Dr. Ivan Guilhon and Dr. Sandro Martini for fruitful discussions and revision of the text. This work was funded by the Brazilian agencies FAPESP (Grant No. 2012/50738-3), CAPES (PVE Grant No. 88887.116535/2016-00), and CNPq (Grants No. 306322/2017-0, No. 308742/2016-8, and No. 154636/2016-9). We acknowledge the National Laboratory for Scientific Computing (LNCC/MCTI, Brazil) for providing HPC resources of the SDumont supercomputer.

[1] I. Georgescu and F. Nori, Phys. World **25**, 16 (2012).

[2] P.-I. Schneider and A. Saenz, Phys. Rev. A **85**, 050304(R) (2012).

[3] J. L. O'Brien, G. J. Pryde, A. G. White, T. C. Ralph, and D. Branning, Nature (London) **426**, 264 (2003).

[4] A. Laucht, R. Kalra, S. Simmons, J. P. Dehollain, J. T. Muhonen, F. A. Mohiyaddin, S. Freer, F. E. Hudson, K. M. Itoh, D. N. Jamieson, J. C. McCallum, A. S. Dzurak, and A. Morello, Nat. Nanotechnol. **12**, 61 (2016).
[5] V. Ivády, I. A. Abrikosov, and A. Gali, npj Comput. Mater. **4**, 76 (2018).
[6] L. Gordon, J. R. Weber, J. B. Varley, A. Janotti, D. D. Awschalom, and C. G. Van de Walle, MRS Bull. **38**, 802 (2013).
[7] W. F. Koehl, H. Seo, G. Galli, and D. D. Awschalom, MRS Bull. **40**, 1146 (2015).
[8] G. Tosi, F. A. Mohiyaddin, V. Schmitt, S. Tenberg, R. Rahman, G. Klimeck, and A. Morello, Nat. Commun. **8**, 1 (2017).
[9] A. K. Geim and I. V. Grigorieva, Nature (London) **499**, 419 (2013).
[10] K. S. Novoselov, A. Mishchenko, A. Carvalho, and A. H. Castro Neto, Science **353**, aac9439 (2016).
[11] Y. Liu, N. O. Weiss, X. Duan, H.-C. Cheng, Y. Huang, and X. Duan, Nat. Rev. Mater. **1**, 16042 (2016).
[12] J. Pawłowski, D. Żebrowski, and S. Bednarek, Phys. Rev. B **97**, 155412 (2018).
[13] S. Khorasani and A. Koottandavida, npj 2D Mater. Appl. **1**, 7 (2017).
[14] S. Khorasani, C—J. Carbon Res. **4**, 39 (2018).
[15] J. I.-j. Wang, D. Rodan-Legrain, L. Bretheau, D. L. Campbell, B. Kannan, D. Kim, M. Kjaergaard, P. Krantz, G. O. Samach, F. Yan, J. L. Yoder, K. Watanabe, T. Taniguchi, T. P. Orlando, S. Gustavsson, P. Jarillo-Herrero, and W. D. Oliver, Nat. Nanotechnol. **14**, 120 (2019).
[16] D. S. Koda, F. Bechstedt, M. Marques, and L. K. Teles, Phys. Rev. B **97**, 165402 (2018).
[17] D. S. Koda, F. Bechstedt, M. Marques, and L. K. Teles, J. Phys. Chem. C **121**, 3862 (2017).
[18] G. Kresse and J. Furthmüller, Phys. Rev. B **54**, 11169 (1996).
[19] G. Kresse and D. Joubert, Phys. Rev. B **59**, 1758 (1999).
[20] J. P. Perdew, K. Burke, and M. Ernzerhof, Phys. Rev. Lett. **77**, 3865 (1996).
[21] J. Klimeš, D. R. Bowler, and A. Michaelides, Phys. Rev. B **83**, 195131 (2011).
[22] H. J. Monkhorst and J. D. Pack, Phys. Rev. B **13**, 5188 (1976).
[23] F. Bechstedt, *Principles of Surface Physics*, Advanced Texts in Physics (Springer, Berlin, 2003).
[24] D. S. Koda, F. Bechstedt, M. Marques, and L. K. Teles, J. Phys. Chem. C **120**, 10895 (2016).
[25] J. Paier, M. Marsman, K. Hummer, G. Kresse, I. C. Gerber, and J. G. Angyán, J. Chem. Phys. **124**, 154709 (2006).
[26] J. Heyd, G. E. Scuseria, and M. Ernzerhof, J. Chem. Phys. **118**, 8207 (2003).
[27] J. Heyd, G. E. Scuseria, and M. Ernzerhof, J. Chem. Phys. **124**, 219906 (2006).
[28] See Supplemental Material at http://link.aps.org/supplemental/10.1103/PhysRevB.100.121406 for additional information on computational details, analysis of the energy separation between the qubit energy eigenstates as a function of the electric field, additional plots of band structures for intermediate electric fields, a prescreening over possible bilayer candidates based on Anderson's rule, a discussion about the conduction by holes at the valence band maximum, and a proposal for multiqubit coupling.
[29] B. Lucatto, L. V. C. Assali, R. R. Pela, M. Marques, and L. K. Teles, Phys. Rev. B **96**, 075145 (2017).
[30] T. Hayashi, T. Fujisawa, H.-D. Cheong, Y. H. Jeong, and Y. Hirayama, Phys. Rev. Lett. **91**, 226804 (2003).
[31] J. Gorman, D. G. Hasko, and D. A. Williams, Phys. Rev. Lett. **95**, 090502 (2005).
[32] B. Schumacher, Phys. Rev. A **51**, 2738 (1995).
[33] G. Cao, H.-O. Li, T. Tu, L. Wang, C. Zhou, M. Xiao, G.-C. Guo, H.-W. Jiang, and G.-P. Guo, Nat. Commun. **4**, 1401 (2013).
[34] R. L. Anderson, IBM J. Res. Dev. **4**, 283 (1960).
[35] T. Roy, M. Tosun, M. Hettick, G. H. Ahn, C. Hu, and A. Javey, Appl. Phys. Lett. **108**, 083111 (2016).